

# Observing the NH<sub>3</sub> snowline in protoplanetary disks with ngVLA

Kenji Furuya,<sup>1</sup> Hideko Nomura,<sup>1</sup> Yuri Aikawa,<sup>2</sup>

<sup>1</sup>*National Astronomical Observatory of Japan, 2-21-1 Osawa,  
Mitaka, Tokyo 181-8588*

<sup>2</sup>*Department of Astronomy, Graduate School of Science, The University of Tokyo, 7-3-1 Hongo,  
Bunkyo-ku, Tokyo 113-0033, Japan  
kenji.furuya@nao.ac.jp*

## Abstract

The snowline is the boundary where molecules freeze-out/sublimate in a protoplanetary disks. The elemental compositions of gas and solid (ice + dust) change significantly across the snowlines of major volatiles such as H<sub>2</sub>O, NH<sub>3</sub>, CO, etc., Then the detection of the snowlines and revealing the compositional changes across the snowlines are essential for understanding planetary composition. In this article, we discuss the observability of the NH<sub>3</sub> snowline in Class II protoplanetary disks with ngVLA. NH<sub>3</sub> is a key species to trace the chemical evolution of nitrogen during star- and planet formation and is also useful as a proxy to trace the H<sub>2</sub>O snowline. We find that the NH<sub>3</sub> snowline is detectable in a disk around a Herbig Ae/Be star with ngVLA, while the detection is challenging for a disk around a T-Tauri star.

**Key words:** protoplanetary disks — ISM: molecules — ISM: abundances

## 1. Introduction

Ammonia (NH<sub>3</sub>) is one of the major reservoirs of nitrogen in star-forming regions, accounting for  $\sim 10\%$  of overall nitrogen (e.g., Öberg et al. 2011). The significant fraction of remaining nitrogen is likely present as N<sub>2</sub> (e.g., Furuya et al. 2018), which is not directly observable. As N<sub>2</sub> is more volatile and chemically stable than NH<sub>3</sub>, NH<sub>3</sub> could be a raw material of N-bearing complex organic molecules (Daranlot et al. 2012), including amino acids. Taken together, NH<sub>3</sub> is a key species to trace the chemical evolution of nitrogen during star- and planet formation.

The bulk of NH<sub>3</sub> in star-forming regions forms in molecular clouds and cores as ice. The NH<sub>3</sub> evolution in the later stages of star-formation, i.e., after protostellar formation, is still largely unknown due to the lack of high spatial resolution observations at cm wavelengths, where NH<sub>3</sub> has rotation-inversion transitions. Gas-phase NH<sub>3</sub> has been detected in the warm ( $>100$  K) gas of a deeply embedded protostellar source with VLA (Choi et al. 2010), where NH<sub>3</sub> ices have sublimated. To the best of our knowledge, there is only one detection of NH<sub>3</sub> in class II protoplanetary disks in the literature (Salinas et al. 2016). The observed gas-phase NH<sub>3</sub> by the *Herschel Space Observatory* traces the cold outer regions of the disk, where only a fraction of NH<sub>3</sub> ice desorbs via photodesorption. In order to trace the bulk NH<sub>3</sub> in disks, the observations of gas-phase NH<sub>3</sub> inside the NH<sub>3</sub> snowline is necessary. It is known that NH<sub>3</sub> is poor in cometary ices with the abundance ratio of NH<sub>3</sub>/H<sub>2</sub>O  $\lesssim 1\%$  (Mumma & Charnley 2011 and references therein), which is much lower than that in interstellar ices,  $\sim 5\%$  (e.g., Öberg et al. 2011). Recent detection of ammonium salts in comet 67P/Churyumov-Gerasimenko by the ROSINA instrument on Rosetta (Altwegg et al. 2020) implies that NH<sub>3</sub> is largely converted into ammonium salts during star- and planet-formation.

ngVLA is the unique instrument that allows us to detect NH<sub>3</sub> inside its snowline and thus to reveal the NH<sub>3</sub> evolution.

NH<sub>3</sub> would be also useful to locate the water snowline in protoplanetary disks. The detection of water snowline by observing water emission lines with ALMA would be challenging, if the inner disk regions, where water snowline locates, are optically thick for dust continuum at mm wavelengths (e.g., Banzatti et al. 2015). Even when dust continuum is optically thick at mm wavelengths, it is likely optically thin at cm wavelengths. In addition, laboratory experiments of the sublimation of interstellar/cometary ice analogs have shown that at least significant fraction of NH<sub>3</sub> ice sublimates together with H<sub>2</sub>O ice (Martín-Doménech et al. 2014). Then, NH<sub>3</sub> is suggested to be a good proxy to trace the water snowline (e.g., Zhang et al. 2018).

## 2. Sensitivity estimate

Here we discuss the observability of the NH<sub>3</sub> snowline in a Class II protoplanetary disk with ngVLA. For this sake, we conduct the line radiation transfer calculations, using a genetic disk model.

### 2.1. Numerical setup

For the physical and chemical structures of a disk, we consider a disk around a Herbig Ae/Be star with the mass of  $2 M_{\odot}$ . We adopt the simulation results from Furuya et al. (in prep.), in which the viscous evolution of gas, the dust evolution (collisional growth and radial drift), and gas-phase and grain surface chemistry are considered in a time-dependent manner. In this 1D radial model, temperature is calculated from the balance between heating by stellar irradiation and viscous dissipation and radiative cooling, using initial disk conditions. The initial disk gas mass is  $0.05 M_{\odot}$  with the dust-to-gas mass ratio of  $\sim 0.01$ . The binding energy of NH<sub>3</sub> is set to be the same as that

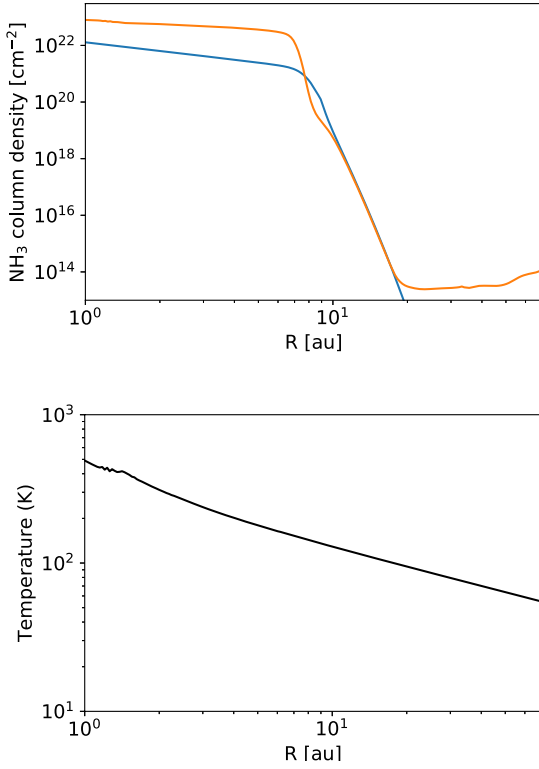


**Fig. 1.** Upper panel) Column density of gas-phase  $\text{NH}_3$  as a function of the distance from the central star in the disk model at  $t = 0$  yr (blue line) and  $3 \times 10^5$  yr (orange line). Lower panel) Temperature distribution in the disk model.

of  $\text{H}_2\text{O}$ , so that the snowlines of  $\text{NH}_3$  and  $\text{H}_2\text{O}$  are co-located in the disk model. It is assumed that the initial chemical composition of the disk is similar to that of dense molecular clouds for simplicity, with the total (gas+ice) initial  $\text{NH}_3$  abundance of  $\sim 10^{-5}$  with respect to hydrogen nuclei, corresponding to the  $\text{NH}_3/\text{H}_2\text{O}$  abundance ratio of  $\sim 10\%$ .

The upper panel of Figure 1 shows that the column density distribution of gas-phase  $\text{NH}_3$  in the model at  $t = 0$  yr and at  $3 \times 10^5$  yr, while the lower panel shows the temperature distribution adopted in the simulations. We chose the two specific time to explore the impact of the  $\text{NH}_3$  column density distribution on the  $\text{NH}_3$  emission. The  $\text{NH}_3$  column density sharply increases at  $\sim 10$  au, corresponding to the snowline of  $\text{NH}_3$ . The  $\text{NH}_3$  column density inside the snowline is higher at the later time, because of the radial drift of ice-coated dust grains and sublimation of  $\text{NH}_3$  ice at the snowline. Outside the  $\text{NH}_3$  snowline, the majority of  $\text{NH}_3$  is present as ice coatings of dust grains, but some amount of  $\text{NH}_3$  still exist in the gas-phase due to the gas-phase chemistry, which converts  $\text{N}_2$  to  $\text{NH}_3$ , and photodesorption of  $\text{NH}_3$  ice. The  $\text{NH}_3$  column density outside the snowline also increases with time, because the total surface area of dust grains, which allows freeze-out of gas-phase  $\text{NH}_3$ , reduces with time due to the coagulation and radial drift of dust grains.

Figure 2 shows that the optical depth for dust continuum at 1 mm and at 1.3 cm in the disk model. The sharp increases of the dust optical depth is seen at  $\lesssim 5$  au, corresponding to

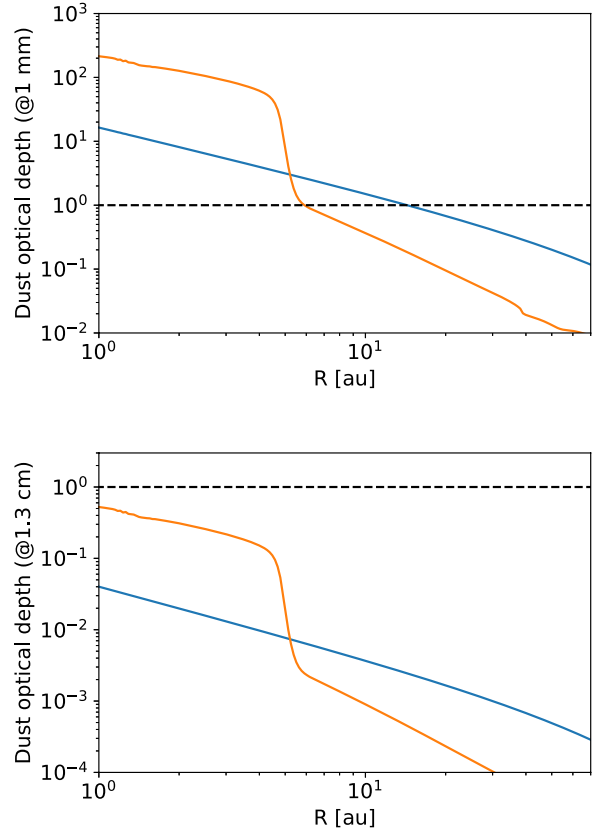


**Fig. 2.** Dust optical depth at 1 mm (upper panel) and at 1.3 cm (lower panel) as a function of the distance from the central star in the disk model at  $t = 0$  yr (blue line) and  $3 \times 10^5$  yr (orange line).

the accumulation of dust grains there. This is caused by the assumption that the threshold fragmentation velocity of bare dust grains is lower than that of dust grains coated by more than one monolayer of water ice (e.g., Banzatti et al. 2015). The dust opacity is calculated with the `dsharp_opac` package (Birnstiel et al. 2018), assuming the minimum and maximum dust sizes of  $0.005 \mu\text{m}$  and  $1 \text{ mm}$ , respectively, with the power law of  $-3.5$ . The dust absorption coefficients are  $2.7 \text{ cm}^2/\text{g}$  at 1 mm and  $6.6 \times 10^{-3} \text{ cm}^2/\text{g}$  at 1.3 cm, respectively, in our models. Dust continuum at 1 mm wavelength (300 GHz) is optically thick at  $\lesssim 10$  au, while at 1.3 cm wavelength (23 GHz), the dust continuum is optically thin in the whole region in the disk. This comparison demonstrates that ngVLA is suitable to observe molecular lines from the midplane of the inner disk regions.

As the adopted disk structure model is a 1D radial model, we have to assume the vertical disk structure. For simplicity, we assume that gas is vertically isothermal, the gas distribution is in the hydrostatic equilibrium, the dust-to-gas mass ratio is vertically uniform (but not uniform radially), and  $\text{NH}_3$  gas is present only below one scale height of the gas. In reality, the distribution of  $\text{NH}_3$  gas inside the snowline would depend on the vertical temperature structure and the strength of vertical mixing. Such details are beyond the scope of this article.

The line radiation transfer calculations of para- $\text{NH}_3$  inversion transitions are performed with LIME (Brinch &

Hogerheijde 2010), assuming local thermal equilibrium (LTE). Molecular data are taken from the Leiden Atomic and Molecular Database (LAMBDA; Schöier et al. 2005). The assumption of LTE is valid as we focus on inner disk midplane, where the gas density is very high ( $>10^{10} \text{ cm}^{-3}$ ). For simplicity, we neglect hyper-fine structures of  $\text{NH}_3$  transitions here, which should be explored in the future work. We assume that the distance of the disk from the Earth is 140 pc and the inclination angle of the disk is  $30^\circ$ .

## 2.2. Results

We performed the line transfer calculations to predict emission in (1,1)-(5,5) rotation-inversion transitions at 23-25 GHz for two snapshots ( $t = 0 \text{ yr}$  and  $3 \times 10^5 \text{ yr}$ ) of the disk structure model. We found that the results for the two snapshots are similar, and thus we here only show the results at  $t = 3 \times 10^5 \text{ yr}$ . The left panel of Figure 3 shows the moment 0 map of the  $\text{NH}_3(5, 5)$  emission model obtained by LIME with the spatial resolution of  $0.004''$  per pixel, while the right panel shows the moment 0 map of the emission model convolved with the  $0.1''$  Gaussian beam. As the intensity sharply drops at the snowline position, one can locate the snowline from the moment 0 map if the spatial resolution is high enough ( $\ll 10 \text{ au}$ ). Considering the sensitivity of ngVLA for line observations, the beam size of  $\sim 0.1''$  ( $\sim 14 \text{ au}$  in our simulations) would be the minimum for the detection of  $\text{NH}_3$  inversion transitions with reasonable observing time (see below). Then, the  $\text{NH}_3$  snowline would be only marginally resolved.

Even when the snowline is not spatially resolved, one can constrain the snowline location from the spectrally resolved observations (e.g., Notsu et al. 2017). Figure 4 shows the spectral of the  $\text{NH}_3(5,5)$  emission extracted from inner  $\sim 20 \text{ au}$ . The peak brightness temperature is  $\sim 50 \text{ K}$ . Then, assuming a beam size of  $0.1''$  and velocity resolution of  $1 \text{ km/s}$ , we can detect the emission with  $\gtrsim 10 \sigma$  ( $\gtrsim 5 \sigma$ ) for 10 hour (2.5 hour) integration time to locate the  $\text{NH}_3$  snowline (cf. <https://ngvla.nrao.edu/page/performance>). We do not see significant difference between (5,5) and (1,1) transitions (Fig. 4), although the upper energy levels are very different (295 K versus 23 K). A higher transition would be better to avoid blending between the main components and the satellite components (note again that our calculations do not consider hyper-fine structures). As the  $\text{NH}_3$  emission from inside the snowline is optically thick, it is hard to constrain the  $\text{NH}_3$  column density. The observations of rarer isotopologues,  $^{15}\text{NH}_3$ , spectrally resolving the hyperfine components, may be helpful to constrain the column density.

In our calculations, we consider a disk around a Herbig Ae/Be star. The detection of the  $\text{NH}_3$  snowline in a T-Tauri disk would be challenging due to the smaller size of the  $\text{NH}_3$  snowlines (at  $\sim 1 \text{ au}$ ) (Zhang et al. 2018).

## 3. Conclusion

In this article, we discussed the observability of the  $\text{NH}_3$  snowline in a Class II protoplanetary disk. We performed the line radiation transfer of rotation-inversion transition of  $\text{NH}_3$ , using a genetic disk model of Furuya et al. (in prep.). We found that the  $\text{NH}_3$  snowline can be detected in a disk around

a Herbig Ae/Be star with ngVLA with reasonable integration time, while the detection is challenging for a disk around a T-Tauri star. The  $^{14}\text{NH}_3$  emission lines are most likely optically thick. Then the observations of rarer isotopologues,  $^{15}\text{NH}_3$ , would be required to constrain the amount of  $\text{NH}_3$  inside its snowline. This article focuses on  $\text{NH}_3$ , while Furuya et al. disk model predicts that complex organic molecules (COMs), such as  $\text{CH}_3\text{OH}$  and  $\text{CH}_3\text{OCH}_3$ , are accumulated in inner disk regions inside water snowline. These COMs would also be interesting targets for ngVLA.

## References

- Altwegg K. et al., 2020, *Nature Astronomy*, 4, 533  
 Banzatti, A., Pinilla, P., Ricci, L., et al. 2015, *ApJ*, 815, L15  
 Birnstiel, T., Dullemond, C. P., Zhu, Z., et al. 2018, *ApJL*, 869, L45  
 Brinch, C. & Hogerheijde, M. R. 2010, *A&A*, 523, A25  
 Choi, M., Tatematsu, K., Kang, M. 2010, *ApJ*, 723, L34  
 Daranlot, J., Hincelin, U., Bergeat, A., Costes, M., Loison, J. C., Wakelam, V., & Hickson, K. M., 2012, *PNAS*, 109, 10233  
 Furuya, K., Watanabe, Y., Sakai, T., Aikawa, Y., & Yamamoto, S. 2018, *A&A*, 615, L16  
 Martín-Doménech, R., Muñoz Caro, G. M., Bueno, J., & Goesmann, F. 2014, *A&A*, 564, A8  
 Mumma, M., & Charnley, S. B. 2011, *ARA&A*, 49, 471  
 Notsu, S., Nomura, H., Ishimoto, D., Walsh, C., Honda, M., Hirota, T., and Millar, T. J. 2017, *ApJ*, 836, 118  
 Öberg, K. I., Boogert, A. C. A., Pontoppidan, K. M., et al. 2011, *ApJ*, 740, 109  
 Salinas, V. N., Hogerheijde, M. R., Bergin, E. A., et al. 2016, *A&A*, 591, A122  
 Schöier, F. L., van der Tak, F. F. S., van Dishoeck, E. F., & Black, J. H., 2005, *A&A*, 432, 369  
 Zhang, K., Bergin, E. A., Williams, J. P., & Andrews, S. M., arXiv:1810.06604

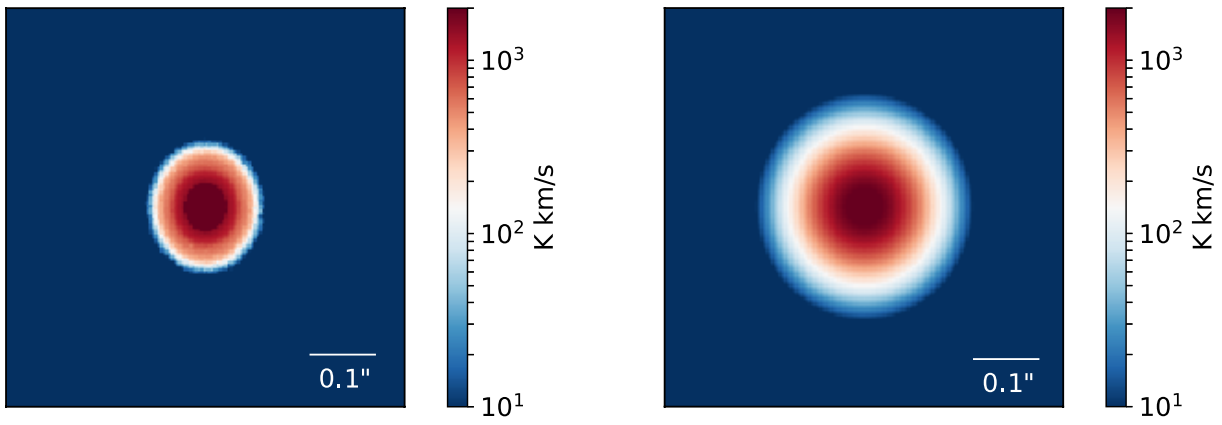


**Fig. 3.** Left panel) Moment 0 map of the  $\text{NH}_3(5, 5)$  emission model obtained by line radiative transfer code LIME. Right panel) The  $\text{NH}_3(5, 5)$  emission model convolved with the  $0.1''$  Gaussian beam.

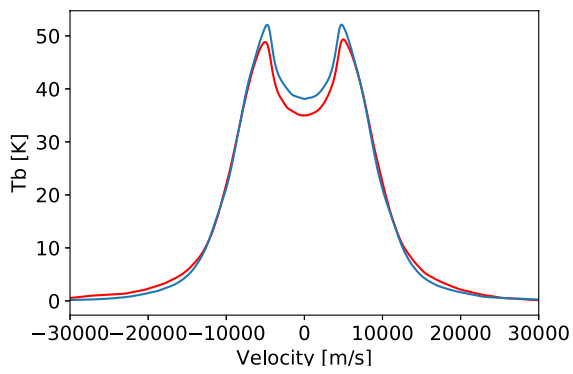


**Fig. 4.** Spectra of the  $\text{NH}_3(1, 1)$  emission (blue line) and the  $\text{NH}_3(5, 5)$  emission (red line).